



# Particle phase state and aerosol liquid water greatly impact secondary aerosol formation: insights into phase transition and its role in haze events

Xiangxinyue Meng<sup>1</sup>, Zhijun Wu<sup>1,2</sup>, Jingchuan Chen<sup>1</sup>, Yanting Qiu<sup>1</sup>, Taomou Zong<sup>1</sup>, Mijung Song<sup>3</sup>, Jiye Lee<sup>4</sup>, and Min Hu<sup>1,2</sup>

<sup>1</sup>State Key Joint Laboratory of Environmental Simulation and Pollution Control, International Joint Laboratory for Regional Pollution Control, College of Environmental Sciences and Engineering, Peking University, Beijing 100871, China

<sup>2</sup>Collaborative Innovation Center of Atmospheric Environment and Equipment Technology, Nanjing University of Information Science and Technology, Nanjing 210044, China

<sup>3</sup>Department of Earth and Environmental Sciences, Jeonbuk National University, Jeonju, 54896, Republic of Korea

<sup>4</sup>Department of Environmental Science and Engineering, Ewha Womans University, Seoul, 03760, Republic of Korea

**Correspondence:** Zhijun Wu (zhijunwu@pku.edu.cn)

Received: 27 September 2023 – Discussion started: 2 November 2023

Revised: 15 January 2024 – Accepted: 18 January 2024 – Published: 26 February 2024

**Abstract.** The particle phase state is crucial for reactive gas uptake, heterogeneous, and multiphase chemical reactions, thereby impacting secondary aerosol formation. This study provides valuable insights into the significance of particle-phase transition and aerosol liquid water (ALW) in particle mass growth during winter. Our findings reveal that particles predominantly exist in a semi-solid or solid state during clean winter days with ambient relative humidity (RH) below 30 %. However, a non-liquid to liquid phase transition occurs when the ALW mass fraction exceeds 15 % (dry mass) at transition RH thresholds of 40 %–60 %. During haze episodes, the transformation rates of sulfate and nitrate aerosols rapidly increase through phase transition and increased ALW by 48 % and 11 %, respectively, resulting in noticeable increases in secondary inorganic aerosols (SIA). The presence of abundant ALW, favored by elevated RH and higher proportion of SIA, facilitates the partitioning of water-soluble compounds from the gas to the particle phase, as well as heterogeneous and aqueous processes in liquid particles. This leads to a substantial increase in the formation of secondary organic aerosols and elevated aerosol oxidation. Consequently, the overall hygroscopicity parameters exhibit a substantial enhancement, with a mean value of 23 %. These results highlight phase transition as a key factor initiating the positive feedback loops between ALW and secondary aerosol formation during haze episodes over the North China Plain. Accurate predictions of secondary aerosol formation necessitate explicit consideration of the particle phase state in chemical transport models.

## 1 Introduction

Submicron particles are ubiquitous in nature, having great impacts on climate, visibility, and human health (Shiraiwa et al., 2011; Ravishankara, 1997; Pöschl, 2005; Lelieveld et al., 2015; Seinfeld et al., 2016; Hu et al., 2021). Phase state, a key parameter of particles, plays profound roles in the mass transport of reactive molecules between the gas phase and the particle phase (Marshall et al., 2018; Shiraiwa et al., 2011). This, in turn, influences the gas–particle partitioning of semi-volatile materials (Shiraiwa et al., 2013; Li and Shiraiwa, 2019), multiphase reaction rates of chemical species (Zhang et al., 2018; Mu et al., 2018), and even the ice-nucleating activities of organic aerosols (OAs) (Murray et al., 2010; Knopf and Alpert, 2023). Aerosol liquid water (ALW) contributes a substantial fraction of the mass in sub-micrometer particles on a global basis (Nguyen et al., 2016). Atmospheric particles with the presence of condensed water serve as suspended vessels of multiphase chemical reactions, leading to significant impacts on secondary aerosol formation, particle size growth, and air quality (Wu et al., 2018; Hodas et al., 2014; Liu et al., 2019). Therefore, a comprehensive understanding of particle phase state and ALW is crucial for better evaluation of the related environmental effects.

In the real atmosphere, the particle phase state varies significantly among solid, semi-solid, and liquid particles under different conditions, which are specifically influenced by ambient relative humidity (RH), temperature, and aerosol chemical composition. For example, the atmospheric particles in the tropical rainforest over central Amazonia, which primarily consisted of secondary organic aerosols (SOAs) derived from oxidation of isoprene, were observed to be in a liquid state at  $\text{RH} > 80\%$  (Bateman et al., 2016), but more non-liquid particles occurred with the impact of anthropogenic pollutants (Bateman et al., 2017). Liu et al. (2019) reported that particles with a high mass fraction of inorganics and high RH were prone to be liquid in a subtropical coastal megacity. However, non-liquid particles appeared at  $\text{RH} < 60\%$  in Beijing (Liu et al., 2017). Moisture can drive an RH-induced glass transition in particles, leading to a liquid state and a significant water uptake at high RH in the lower atmosphere (Mikhailov et al., 2009). Moreover, organic aerosols might be in a solid state at upper tropospheric temperatures that are below about 210 K (Koop et al., 2011). Therefore, the changing features of aerosol composition and ambient RH may alter the ALW and trigger the phase state variation. More studies are needed to clarify the relationship between aerosol composition, particle phase state, and ALW.

After the implementation of “China’s Action Plan for Air Pollution Prevention and Control” in 2013, emissions of primary particulate matter and several gaseous pollutants have greatly reduced. However, the contribution and proportion of secondary inorganic aerosols (SIAs) and SOAs have become increasingly significant (Lei et al., 2021; Y. Wang et al., 2021), especially during haze episodes in winter. As men-

tioned, particles change from solid to liquid with elevated RH conditions during heavy haze episodes (Liu et al., 2017). In liquid particles, the gas–particle mass transfer for reactive gases can be greatly facilitated due to increased diffusion coefficients, and the thermodynamic equilibrium of semi-volatile compounds may be impacted, contributing to secondary aerosol formation (Shiraiwa et al., 2011; Jia et al., 2023). A recent field study by Gkatzelis et al. (2021) pointed out that the gas-to-particle partitioning in liquid particles enhances the uptake of water-soluble gas compounds, resulting in a 15%–25% contribution of SOA mass during particulate pollution in Beijing. Many studies have demonstrated that the abundant ALW and high-RH conditions can greatly impact secondary aerosol formation processes (Xu et al., 2017; J. F. Wang et al., 2021; Gkatzelis et al., 2021). However, there is still a lack of understanding regarding the role of phase state variations in secondary particulate pollution. In this study, we conducted a 1-month field campaign in Beijing during winter to investigate the relationship between particle phase state, ALW, and the chemical and physical processes involved in haze formation.

## 2 Methodology

### 2.1 Instruments and measurements

Field campaigns were conducted in Beijing from 15 December 2020 to 10 January 2021 at the Changping campus of Peking University ( $40^{\circ}8' \text{N}$ ,  $116^{\circ}6' \text{E}$ ). A detailed description of the sampling site can be found in previous studies (Y. Wang et al., 2020b). The instruments were situated in the air monitoring laboratory, located on the top floor of the main building. A weather station (Met One Instruments Inc., USA), a suite of automatic gas analyzers ( $\text{O}_3$ ,  $\text{SO}_2$ ,  $\text{CO}$ , and  $\text{NO}_x$ ) from Thermo Scientific, and an Aerodyne Quadrupole Aerosol Chemical Speciation Monitor (Q-ACSM) were operated according to standard protocols (Ng et al., 2011) and necessary information as described in Sect. S1 in the Supplement.

The particle rebound fraction ( $f$ ) was measured using a modified three-arm impactor (Bateman et al., 2014) coupled to a condensation particle counter (CPC; model 3772, TSI Inc.) with a time interval of 3 min, as described in our previous work (Liu et al., 2017; Meng et al., 2021). The three-arm impactor consisted of three parallel impactors with different designs. One of the impactors had no plate, while the others had plates equipped with an uncoated plate and a grease-coated plate, respectively. The no-plate impactor provided the total throughput rate, while the solid surface of the uncoated plate let particles rebound, and the sticky surface of the grease-coated plate captured all particles that struck it. To measure the  $f$ , a valve system with three solenoids and two actuators was used to ensure that the particle populations passing through the three impactors were sequenced and were measured by the CPC. Thus, the rebound fraction,

$f$ , was defined as

$$f = \frac{N_2 - N_3}{N_1 - N_3}, \quad (1)$$

where  $N_1$  was the whole particle population,  $N_2$  was the population of particles that did not strike in addition to the rebounded particles from the impaction plate, and  $N_3$  was the population of particles that did not strike the impaction plate. Prior to measurement, we dried the particles to below 30 % RH using a silica gel diffusion dryer. Then, 300 nm monodisperse particles were selected by a differential mobility analyzer (DMA; TSI model 3080). An RH adjustment system with two RH probes and a Nafion RH conditioner was employed to measure the RH conditions (ambient RH and impactor RH), as well as to adjust the impactor RH to match the real atmospheric RH. The measured impactor RH rapidly reached the ambient RH within 1 s, exhibiting a mean absolute error of 0.03. This swift regulation time is attributed to the real-time feedback in the RH control system, coupled with the typically modest fluctuations in ambient RH. Particles with a diameter of 300 nm, as selected for our study, rapidly achieved equilibrium in the humidification process, since the timescale for water diffusion into these particles is approximately 1 s, shorter than their residence time of about 3 s within the system. This is detailed in Sect. S2 and illustrated in Fig. S1. Such conditions ensure that the measured particle rebound is representative and accurate at ambient RH. Weekly calibrations using standard ammonium sulfate and a daily flow check were conducted (Liu et al., 2021, 2019). Typically,  $f < 0.2$  or 0.1 refers to the complete phase transition from a non-liquid to a liquid state (Pajunoja et al., 2016; Liu et al., 2017). In this study, we consider  $f < 0.2$  in the case of a liquid state. The time series of  $f$  with an initial time resolution is shown in Fig. 1, while the data presented in other figures are all displayed as hourly averages.

## 2.2 Data analysis

The mass concentrations of organics, sulfate, nitrate, ammonium, and chloride in non-refractory particles (NR-PM<sub>1</sub>) were analyzed using the standard ACSM data analysis software (v.1.5.10). A collection efficiency (CE) of 0.5 was applied to the dataset (Xu et al., 2017; Matthew et al., 2008). Positive matrix factorization (PMF) was performed on the organic mass spectra using the Igor Pro-based PMF2.exe algorithm to resolve primary organic aerosol (POA) and SOA factors. The data and error matrices were pretreated following methods from previous studies (Zhang et al., 2011, 2017). The key diagnostic plots are provided in the Supplement (Figs. S2 and S3).

The aerosol liquid water content contributed by inorganics (ALW<sub>inorg</sub>) in PM<sub>1</sub> was estimated using the ISORROPIA-II thermodynamic model (Fountoukis and Nenes, 2007) with input of aerosol chemical composition measured by Q-ACSM. The particles were assumed to be in a metastable

state, and the reverse mode was used to calculate the ALW<sub>inorg</sub> due to the absence of gaseous HNO<sub>3</sub> and NH<sub>3</sub>. Besides, ALW associated with organics (ALW<sub>org</sub>) was considered using a simplified equation of  $k$ -Köhler theory (Guo et al., 2015; Petters and Kreidenweis, 2007):

$$\text{ALW}_{\text{org}} = V_{\text{org}} k_{\text{org}} \frac{a_w}{1 - a_w}, \quad (2)$$

where  $V_{\text{org}}$  is the volume concentration of organics with a typical density of 1.4 g cm<sup>-3</sup> (Cerully et al., 2015);  $k_{\text{org}}$  is the hygroscopicity parameter of the organics; and  $a_w$  represents the water activity, which is assumed to have the same value as RH. In this study, we used a fixed  $k_{\text{org}}$  of 0.06 to evaluate ALW<sub>org</sub>, which was the average value of the overall  $k_{\text{org}}$  in the consideration of POA and SOA contributions in the total non-refractory organics ( $k_{\text{POA}} = 0$  and  $k_{\text{SOA}} = 0.1$ ) (Wu et al., 2016; Gunthe et al., 2011). However, it should be noted that  $k_{\text{org}}$  has been found to exhibit a positive linear relationship with the aerosol oxidation degree, which varied among species (Chang et al., 2010; Duplissy et al., 2011).  $f_{44}$ , the fraction of  $m/z$  44 fragment signal to total organic signal, is widely used to represent the atmospheric aging process of OA species (Ng et al., 2010; Canagaratna et al., 2015). Real-time  $k_{\text{org}}$  was  $k_{\text{org}} = 1.04 \times f_{44} - 0.02$ , as reported by Kuang et al. (2020) for the North China Plain (NCP). The predicted real-time  $k_{\text{org}}$  ranged from 0.13 to 0.24, which was consistent with the variation range reported for winter Beijing (0.06–0.3) (Li et al., 2019; Jin et al., 2020). For fixed  $k_{\text{org}}$ , the contribution of organics to ALW was  $\sim 12\%$  on average during the observation. However, considering the variation of real-time  $f_{44}$ , organics were capable of providing more than 30 % and 20 % of the total ALW mass on average during clean and polluted days, respectively (Fig. S4). In recognition of ALW's plasticizing effect on particle phase state, the potential impacts of whether the hygroscopicity value of organics is fixed or varies in real time on phase transition have been discussed in Sect. 3.2.

For a given internal mixture, the overall particle hygroscopicity ( $k_{\text{total}}$ ) was calculated by a simple mixing rule by weighting the hygroscopicity parameters of the components by their volume fractions in the mixture (Petters and Kreidenweis, 2007):

$$k_{\text{total}} = k_{\text{inorg}} \cdot \text{frac}_{\text{inorg}} + k_{\text{org}} \cdot \text{frac}_{\text{org}}, \quad (3)$$

where  $\text{frac}_{\text{inorg}}$  and  $\text{frac}_{\text{org}}$  are the inorganics and organics volume fractions in NR-PM<sub>1</sub>, respectively. Considering the variability in the composition of inorganics and organics, the hygroscopicity parameters of inorganics ( $k_{\text{inorg}}$ ) were weighted by volume fractions. The main form of inorganic species (NH<sub>4</sub>NO<sub>3</sub> and (NH<sub>4</sub>)<sub>2</sub>SO<sub>4</sub>) in the urban atmosphere was considered due to the lower abundance of chloride in NR-PM<sub>1</sub>. The volume fraction of each inorganic species was calculated based on the ion-pairing scheme as described in Gysel et al. (2007) with their gravimetric density (1720 kg m<sup>-3</sup> for NH<sub>4</sub>NO<sub>3</sub> and 1769 kg m<sup>-3</sup> for

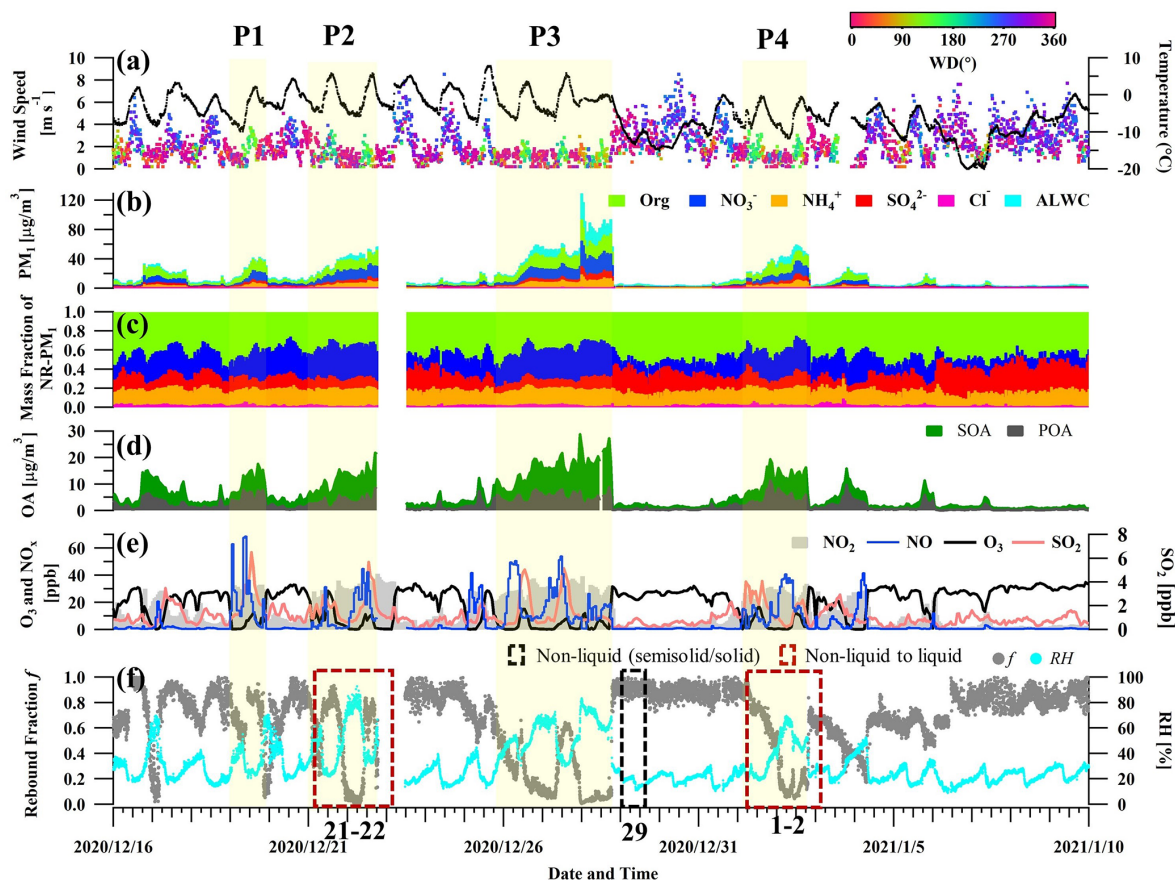


**Figure 1.** Time series of (a) wind speed (WS), wind direction (WD) and temperatures; (b) mass concentration of NR-PM<sub>1</sub> and ALW; (c) mass contribution of NR-PM<sub>1</sub>; (d) mass concentrations of SOA and POA; (e) concentrations of gas pollutants (NO<sub>2</sub>, NO, O<sub>3</sub>, and SO<sub>2</sub>); and (f) rebound fraction and ambient RH during the field campaign. In panel (f), the black (red) frame with the dashed line represents the non-liquid state (transition from non-liquid to liquid state) of bulk PM<sub>2.5</sub> droplets based on offline viscosity measurement using a poke-and-flow technique (Song et al., 2022).

(NH<sub>4</sub>)<sub>2</sub>SO<sub>4</sub> (Wu et al., 2016). The hygroscopicity parameters of NH<sub>4</sub>NO<sub>3</sub> and (NH<sub>4</sub>)<sub>2</sub>SO<sub>4</sub> are 0.58 and 0.48, respectively, following previous studies (Wu et al., 2016; Jin et al., 2020; Petters and Kreidenweis, 2007). For hygroscopicity parameters of organics ( $k_{\text{org}}$ ), real-time  $k_{\text{org}}$  values were used as above, which effectively captured the characteristics of the investigated area in our study.

### 3 Results and discussion

#### 3.1 Chemical composition and phase state of sub-micrometer particles

Figure 1 shows the time series of meteorological parameters, chemical composition of NR-PM<sub>1</sub>, gas pollutants, and particle rebound fraction from 16 December 2020 to 10 January 2021. The average mass concentration of NR-PM<sub>1</sub> was  $15.8 \pm 16.8 \mu\text{g m}^{-3}$  during the measurement period. During clean periods (NR-PM<sub>1</sub> <  $20 \mu\text{g m}^{-3}$ ), organics dominated the aerosol composition, accounting for  $\sim 45\%$  of NR-

PM<sub>1</sub> mass. Nitrate, sulfate, and ammonium contributed 20 %, 16 %, and 16 % to total NR-PM<sub>1</sub> on average, respectively (Fig. S5). However, several pollution episodes occurred, with rapid growth in NR-PM<sub>1</sub> and ALW mass concentration with higher concentrations of NO<sub>x</sub> and SO<sub>2</sub>, as marked by yellow shading in Fig. 1. These four polluted episodes typically started with ambient RH below 40 % and higher O<sub>3</sub> levels (> 30 ppb) and mounted up with stagnant meteorological conditions, bringing high RH (> 60 % RH) and low surface wind speed (<  $3 \text{ m s}^{-1}$ ). This meteorological pattern is commonly observed over the NCP during haze episodes (Sun et al., 2013, 2015). During these polluted episodes, nitrate increased rapidly accounting for an average of 33 % of the total NR-PM<sub>1</sub> mass. ALW was minor during clean days but increased up to 26 % in PM<sub>1</sub> during severe polluted episodes with NR-PM<sub>1</sub> >  $80 \mu\text{g m}^{-3}$  (Fig. S6). The mass concentrations of POA and SOA both increased during these polluted episodes, as shown in Fig. 1d. Moreover, the mass contribution of SOA to total OA showed an upward trend in particu-

late mass, indicating the important contribution of secondary formation during haze formation (Fig. S7).

As shown in Fig. 1f, particle rebound fraction,  $f$ , varied with ambient RH from 1.0 to  $\sim 0.0$  during the observation, indicating that particles possessed a phase transition from a non-liquid to a liquid state. Similar patterns of particle-phase transition were found for several polluted episodes. Taking P4 as an example,  $f$  remained stable at 0.8 with  $\text{RH} = \sim 20\%$  during the initial period of stagnant conditions but gradually dropped to  $\sim 0.1$  along with the increasing RH and NR-PM<sub>1</sub> during the subsequent haze formation. In addition, we collected several PM<sub>2.5</sub> filter samples to characterize the bulk-phase viscosity during clean and polluted days based on a poke-and-flow experiment, as described in our previous study (Song et al., 2022) and Sect. S4 (indicated by black and red frames in Fig. 1f). As shown in Fig. S8, the viscosity was proved to be higher than  $\sim 10^8$  Pa s, with a mean value of  $f > 0.8$  during clean days, indicating that particles existed in a solid or semi-solid state. However, the viscosity was lower than  $\sim 10^2$  Pa s, with an average  $f < 0.2$  under higher RH conditions during polluted days, indicating a liquid state. It should be noted that the viscosity measurement captured the bulk-phase viscosity for water soluble components in PM<sub>2.5</sub> filter samples, but the on-line measurement of  $f$  depicted 300 nm particles representative of accumulation-mode particles, which normally contributed the majority fraction of PM<sub>1</sub>. While the differences in chemical composition between PM<sub>2.5</sub> filter samples and 300 nm particles may introduce uncertainties when comparing the phase state of the targeted aerosols, the viscosity results showed good agreement with the average variation of  $f$  during the corresponding period. Further validation is still necessary to compare the two different techniques and will be displayed in our further study. To directly indicate the phase transition from the perspective of viscosity, RH-dependent  $f$  was measured for these filter samples with known bulk-phase viscosity (Sect. S5 and Fig. S9). As expected, the decreasing  $f$  from  $> 0.8$  to 0 covered the transition range from  $\sim 10^8$  to  $\sim 10^2$  Pa s, which indicated the consistent behavior of particle rebound and measured bulk-phase viscosity for the investigated aerosols.

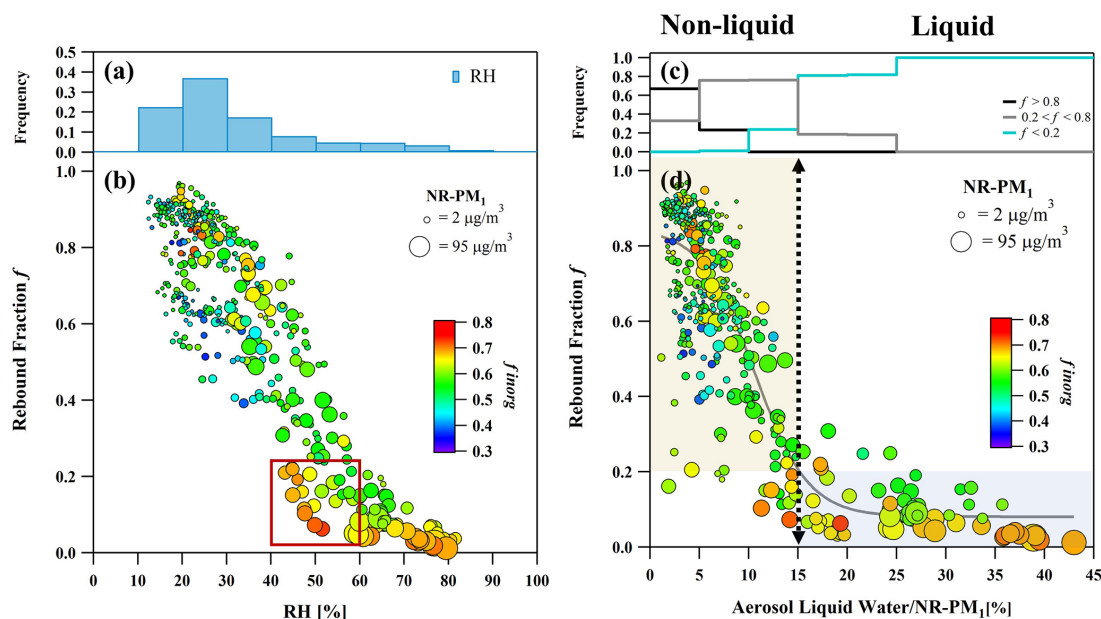
### 3.2 Phase transition behavior of sub-micrometer particles

Figure 2a illustrates the frequency distribution of RH.  $f$  as a function of RH is plotted in Fig. 2b. During the observation, ambient RH was below 30% for more than half of the time, with  $f$  predominantly exceeding 0.8 under such conditions. When RH increased to  $\sim 50\%$ – $60\%$ , the majority of  $f$  dropped to  $< 0.2$  along with the increasing NR-PM<sub>1</sub> mass. This means that particles went through a moisture-induced phase transition from non-liquid to liquid during haze formation when RH reached 60%, which aligned with our previous studies (Liu et al., 2017). Notably, some points with higher

mass fraction of inorganics ( $f_{\text{inorg}} > 0.7$ ) showed  $f < 0.2$  at  $\text{RH} = 40\%$ – $50\%$ , indicating that particles with higher  $f_{\text{inorg}}$  were already in a liquid state. Consequently, particles underwent phase transition with a relatively large RH range of 40%–60%, exhibiting varying chemical compositions, as marked by the red frame.

Particle phase state is known to be sensitive to ALW by its unique plasticizer effect (Koop et al., 2011). In Fig. 2d,  $f$  as a function of ALW / NR-PM<sub>1</sub> is plotted to represent the relative water uptake of unit mass dry aerosols with corresponding particle rebound behaviors. Figure 2c displays the frequency distribution of three  $f$  intervals in each ALW / NR-PM<sub>1</sub> bin. When ALW / NR-PM<sub>1</sub>  $< 5\%$ , the frequency of  $f > 0.8$  was higher than 0.65, indicating that particles mostly stay in a more viscous non-liquid state with less water uptake capacity. When ALW / NR-PM<sub>1</sub> increased to 5%–15%,  $f$  gradually decreased from 0.8 to 0.2, suggesting that the total water uptake gradually enhanced and lowered the viscosity to trigger the phase transition within this range. The non-liquid particles were dominant with the frequency of  $f = 0.2$ – $0.8$  close to 0.8. When ALW / NR-PM<sub>1</sub>  $> 15\%$ , the frequency of  $f < 0.2$  dramatically increased from 0.2 to  $\sim 0.8$ , reaching close to 1.0 at ALW / NR-PM<sub>1</sub>  $> 25\%$  with higher particulate mass. This indicates that particles mostly convert to liquid when the mass fraction of ALW surpasses a certain threshold during haze formation, rather than the absolute ALW mass (Fig. S10). In general, a good correlation between ALW / NR-PM<sub>1</sub> and  $f$  was observed. ALW / NR-PM<sub>1</sub>, used as a mass-based hygroscopic growth factor (Chen et al., 2022; Liu et al., 2018), is suitable to quantify the moisture-induced phase transition capacity of atmospheric particles, and a value of 15% can be the sudden change in the case of phase transition from non-liquid to liquid.

It should be noted that calculations of ALW in this study have considered inorganic salts and organics. Acknowledging that the hygroscopicity of organics, characterized by either a fixed  $k_{\text{org}}$  or varying in real-time, affects the calculation of ALW mass, a sensitivity analysis examining its impact on the phase transition threshold (ALW / NR-PM<sub>1</sub>) is presented in Fig. S11. There is no denying that the contribution of inorganic salts to ALW remains predominant, with their contribution to ALW being  $\sim 88\%$  (a fixed  $k_{\text{org}}$  of 0.06) and  $\sim 73.5\%$  (real-time  $k_{\text{org}}$ ) on average during the observation (Fig. S4), indicating that the impact of different ALW calculations on ALW / NR-PM<sub>1</sub> values was minor. As expected, the frequency distribution of these three  $f$  intervals showed no obvious change for ALW calculations by inorganics, fixed  $k_{\text{org}}$ , and real-time  $k_{\text{org}}$  for the whole ALW / NR-PM<sub>1</sub> range. Although the frequency of  $f < 0.2$  changed from  $\sim 0.8$  to 0.5 at ALW / NR-PM<sub>1</sub> = 15%–20%, when shifting to real-time  $k_{\text{org}}$ , the frequency remained higher than 0.5 and approached 1.0 with larger ALW / NR-PM<sub>1</sub> values. This indicates that while the varying  $k_{\text{org}}$  impacts the number of data points within ALW / NR-PM<sub>1</sub> bins of 15%–20%, it does not affect the overall transition trend. As a result, the impacts of



**Figure 2.** The frequency distribution of ambient RH in each RH bin (a) and the frequency distribution of each  $f$  interval in each ALW / NR-PM<sub>1</sub> bin (c). Rebound fraction  $f$  as a function of ambient RH (b) and ALW / NR-PM<sub>1</sub> (d) during the observation. In panels (b) and (d), the scatter points are colored by  $f_{\text{inorg}}$  in NR-PM<sub>1</sub>, and the point size is scaled by NR-PM<sub>1</sub> mass concentration. The yellow shading and blue shading represent the non-liquid and liquid phase, respectively.

different ALW calculation on ALW / NR-PM<sub>1</sub> were not significant, and the phase transition threshold of 15% remains valid. It is suggested that caution should be exercised when using the above approach to characterize the phase state of targeted aerosols, as the measured  $f$  was representative of accumulation-mode particles that dominated the mass concentration of sub-micrometer particles (Seinfeld and Pandis, 2006).

It is interesting to note that several points with ALW / NR-PM<sub>1</sub> < 5% and NR-PM<sub>1</sub> > 30  $\mu\text{g m}^{-3}$  exhibited a lower rebound fraction ( $f < 0.4$ ), which was attributed to the variation of RH background from high RH to low RH during the later stages of the haze episodes, as shown in Figs. 2d and S12. This suggests that liquid particles may not turn to be a more viscous semi-solid state in a brief period of dehydration. There are two possible explanations for this phenomenon. Firstly, the presence of significant amounts of inorganic and organic compounds can alter the humidity conditions for deliquescence and efflorescence (Ushijima et al., 2021; Peckhaus et al., 2012). Secondly, these particles are likely to be in a non-ideal mixing scenario due to a drying process that forms a core–shell structure (Shiraiwa et al., 2013; Ciobanu et al., 2009; Song et al., 2013). Studies have revealed that the outer phase may form a viscous organic shell to prevent water evaporation (Koop et al., 2011; Shiraiwa et al., 2013; Hodas et al., 2015); thus, the inner phase containing inorganics still keeps liquid with residual water. However, it should be noted that liquid–liquid phase separation was not optically detected under staged dehydration of

filter-based Beijing PM<sub>2.5</sub> droplets by Song et al. (2022). Instead, they observed abrupt effloresced inorganics at  $\sim 30\%$  RH, which was much lower than  $(\text{NH}_4)_2\text{SO}_4$  and  $\text{NH}_4\text{NO}_3$  in pure form (Peng et al., 2022). This supports the fact that atmospheric particles are only more likely to be metastable after liquefaction if RH decreases to very low values.

In addition to RH and aerosol compositions, environmental temperature also plays a significant role in determining the phase state (Koop et al., 2011; Shiraiwa et al., 2017; Petters et al., 2019). A reduction in temperature results in higher viscosity, whereas a rise in RH leads to a decrease in viscosity, attributed to the plasticizing effect of water (Koop et al., 2011). Although the relationship between  $f$  and temperature is not as strongly evident as that of RH in this study (Fig. S13), it is observed that a greater number of data points exhibited near 0.9 under low-RH conditions (< 30%), suggesting higher viscosity at colder temperatures (<  $-10^\circ\text{C}$ ) than warmer scenarios. The glass transition temperature ( $T_g$ ) is a key metric for the non-equilibrium phase transition from a glassy solid to a semi-solid state as temperature rises (Koop et al., 2011). Particles act as solid when the temperature falls below  $T_g$  ( $T_g/T > 1$ ) and transition to semi-solid or liquid at temperatures exceeding  $T_g$ . An increase in compound molecular weight, O : C ratio, and functional group composition are identified as key factors affecting the  $T_g$  of OA (Saukko et al., 2012; Dette et al., 2014; Rothfuss and Petters, 2017; Shiraiwa et al., 2017). Shiraiwa et al. (2017) proposed that  $T_g/T$  is an indicator for the semi-solid to liquid phase transition of OA, with a threshold of  $T_g/T \approx 0.8$ . In this study, we employed a

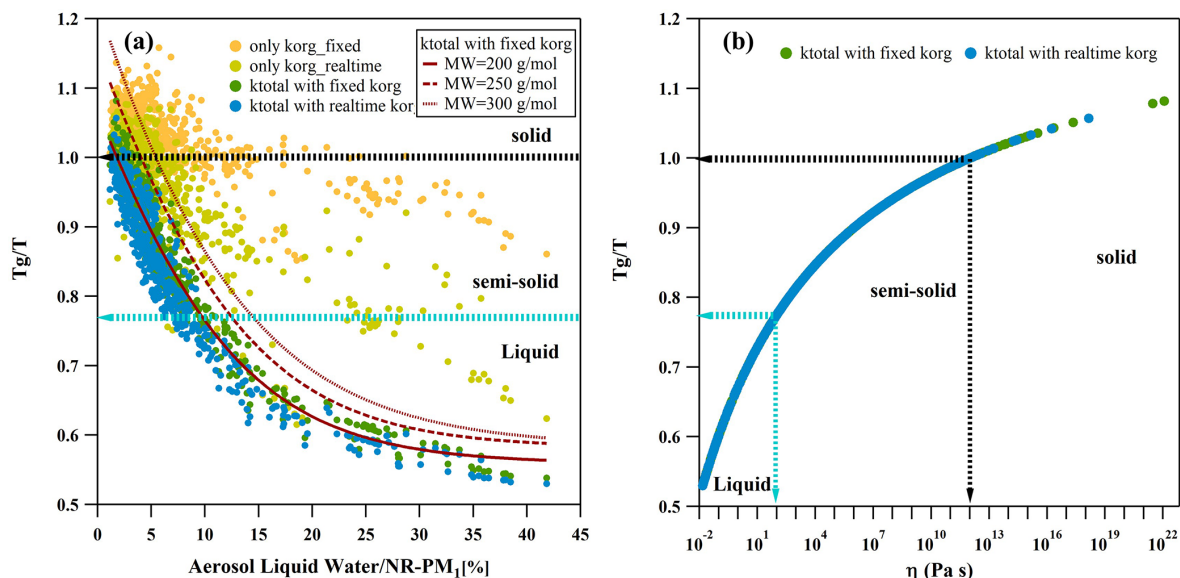
$T_g$  parameterization method for OA viscosity based on their molecular weight and O : C ratio to assess the combined effects of aerosol composition, RH and temperature on particle phase state (Shiraiwa et al., 2017). This method accounts for water associated with both inorganics and organics, rather than focusing solely on organics, to calculate  $T_g$  of ambient OA, as elaborated in Sect. S6.

Figure 3a displays the characteristic relations between  $T_g/T$  and ALW / NR-PM<sub>1</sub>, with a different approach for  $T_g$  calculations of ambient OA. Different phase state intervals are characterized by  $T_g/T$  based on predicted viscosity  $\eta$  as shown in Fig. 3b and are illustrated using dashed lines with arrows. The predicted viscosity  $\eta$  of OA was calculated by applying the Vogel–Tammann–Fulcher (VTF) equation (Angell, 1991) with a fragility parameter of 10 (DeRieux et al., 2018). Clearly, after calculating  $T_g$  in conjunction with  $k_{\text{total}}$ , there is a strong consistency in the characteristic relationship between the estimated  $T_g/T$  and ALW / NR-PM<sub>1</sub> with both fixed and variable  $k_{\text{org}}$ . This consistency aligns well with the phase state changes of atmospheric aerosols discussed earlier in this study. In contrast, even when accounting for variations in hygroscopicity due to different oxidation degrees of OA, the majority of these estimated  $T_g/T$  values fall within the semi-solid and solid range at higher ALW / NR-PM<sub>1</sub>, significantly deviating from the field observations. This highlights the significant impact of environmental RH and chemical composition on the moisture-induced phase transition of atmospheric particles in the near-surface atmosphere. In particular, inorganic salts play a dominant role, contributing more significantly to the mass fraction of ALW in total particulate matter. The estimated  $T_g/T$  for ambient OA with  $k_{\text{total}}$  transitioned to a liquid state at ALW / NR-PM<sub>1</sub> > 10 %, which is slightly lower than the transition threshold of 15 % proposed in this study. It should be noted that the estimated  $T_g$  of OA adopted an average molecular weight (MW) of 200 g mol<sup>-1</sup>, as used in previous studies (Williams et al., 2010; Shen et al., 2018). However, the average MW of ambient OA is likely variable due to the atmospheric aging process. Increasing the value of MW can shift the characteristic curve of  $T_g/T$  versus ALW / NR-PM<sub>1</sub> to the right, thereby aligning the semi-solid to liquid transition threshold more closely with the results observed in this study. This further suggests that incorporating  $k_{\text{total}}$  into  $T_g$  calculation may potentially enhance the simulation results, especially in regions with a high proportion of inorganic salts under humid conditions. It should be noted that this aspect warrants further exploration in subsequent research.

### 3.3 Effects of phase transition and ALW on SIA formation during haze episodes

We investigated the  $f$  and secondary aerosols during four polluted episodes (P1 to P4) under stagnant weather conditions with WS < 3 m s<sup>-1</sup>. Sulfur and nitrogen oxidation ratios, SOR (nSO<sub>4</sub>/(nSO<sub>4</sub>+nSO<sub>2</sub>)) and NOR (nNO<sub>3</sub>/(nNO<sub>3</sub>+nNO<sub>2</sub>)), commonly used as indicators for secondary inorganic transformation (Li et al., 2017), are plotted as a function of  $f$  in Fig. 4a and b. We found that SOR (NOR) remained in a lower level, with a mean value of ~0.27 (0.08) at  $f > 0.2$  for non-liquid particles but increased significantly to ~0.8 (0.35) with increasing ALW / NR-PM<sub>1</sub> at  $f < 0.2$ . This indicates that the secondary formation of SIA is facilitated to a certain degree through phase transition and the increasingly higher ALW mass. It should be noted that particles can be non-liquid during haze episodes with  $f = 1.0$ –0.2. Interestingly, SOR and NOR remained in lower levels and did not show notable increase between  $f = 1.0$ –0.8 and  $f = 0.8$ –0.2, until particles accomplished the phase transition at  $f = 0.2$ –0.0 (Fig. 4c1 and c2). As a result, the median SOR (NOR) increased to higher levels with an increment of 48 % (11 %) via phase transition along with the increase in ALW.

From the perspective of phase state, the increasing mass fraction of ALW reduces the viscosity and triggers the phase transition, which have important roles in the gas–particle mass transfer during haze formation. It is suggested that the secondary transformation of SIA is impeded by limited mass transfer between gas and particle phase when particles are not fully converted into liquid state. However, these limited factors disappear or the dominant formation pathway changes after phase transition. As reported in previous studies, ALW facilitates the secondary formation of sulfate and nitrate via the promotion of heterogeneous reactions (e.g. SO<sub>2</sub> heterogeneous oxidation, N<sub>2</sub>O<sub>5</sub> hydrolysis), gas–particle partitioning of semi-volatile components, or aqueous-phase reactions on wet aerosols (Chen et al., 2022; Cheng et al., 2016; Y. Wang et al., 2020a; Liu et al., 2020). However, aqueous-phase oxidation of SO<sub>2</sub> may be constrained before phase transition due to the low diffusivity of multiple oxidants (e.g. O<sub>3</sub>, H<sub>2</sub>O<sub>2</sub>, and NO<sub>2</sub>) in the particles, and it may become the dominant formation pathway in liquid particles (Ravishankara, 1997; Liu et al., 2020). Additionally, the partitioning of nitrate into particles following Henry's law may also be facilitated by the increased ALW due to enhanced diffusivity of dissolved precursors in liquid particles. In Fig. 4d, the mass fraction of SIA ( $f_{\text{SIA/NR-PM}_1}$ ) is plotted as a function of  $f$ . The  $f_{\text{SIA/NR-PM}_1}$ , ALW mass concentration, and RH were grouped and averaged corresponding to an  $f$  bin width of 10 %. We found that  $f_{\text{SIA/NR-PM}_1}$  remained stable at  $f = 1.0$ –0.4 but steadily increased from an average of ~0.50 to ~0.65 with elevated RH levels (> 40 %) and decreasing  $f$  (from 0.4 to 0.0). This indicates that SIA formation was limited for non-liquid particles with higher viscosity under lower RH conditions. However, ALW was steadily enhanced by the increasing RH, thereby starting to trigger the phase transition and facilitating the SOR and NOR to a larger extent. Therefore,  $f_{\text{SIA/NR-PM}_1}$  apparently increased with the increase in ALW at  $f = 0.2$ –0.0. The presence of more ALW in liquid particles was expected to promote the SIA formation by acting as multiphase reaction



**Figure 3.** Characteristic relations between  $T_g/T$  and ALW / NR-PM<sub>1</sub> (a) and  $T_g/T$  as a function of predicted viscosity  $\eta$  (b) of organic aerosols under ambient conditions. In panel (a), the red curves, which employ sigmoid fitting, represent variations in average molecular weights of OA used for  $T_g$  calculation in consideration of the total hygroscopicity of the particles. The characteristics of the particle phase state are delineated by arrows and dashed lines.

vessels (Zheng et al., 2015; H. Wang et al., 2020; Y. Wang et al., 2020a). One should note that the average environmental temperature during pollution episodes increased to approximately 0 °C, in contrast to the −10 °C recorded during clean periods. The rise in ambient temperature typically enhances the diffusivity of atmospheric reactive molecules in both the gas and particle phases (Tang et al., 2014; Shiraiwa et al., 2011; Li and Shiraiwa, 2019). This, in turn, may potentially influence the heterogeneous or liquid-phase reactions and even the gas–particle partitioning of semi-volatile compounds.

### 3.4 Effects of phase transition and ALW on SOA formation during haze episodes

In Fig. 5a and b, the ratio of SOA to POA (SOA / POA) is plotted as a function of  $f$  during these four polluted episodes characterized by ALW / NR-PM<sub>1</sub> and  $f_{44}$ . For  $f = 1.0$ –0.2, particles possessed relatively lower SOA / POA values (1–2.5) with ALW / NR-PM<sub>1</sub> < 15 %, which was independent of NR-PM<sub>1</sub> mass concentrations. However, a noticeable increase in SOA / POA and elevated  $f_{44}$  values were observed at  $f = 0.2$ –0.0, accompanied by increasing ALW / NR-PM<sub>1</sub> and NR-PM<sub>1</sub> mass. This indicates that more oxidized SOA was produced in liquid particles through the phase transition and the increasing mass fraction of ALW during haze formation. Interestingly, we observed that these liquid particles were primarily associated with polluted days during the nighttime (Fig. S14). For these liquid particles, SOA / POA doubled to  $\sim 5.5$  along with the increasing  $f_{44}$  compared to

non-liquid particles, suggesting the important roles of phase transition and ALW in promoting the SOA formation through dark reactions during nighttime. From the perspective of phase state, phase transition was directly indicated by the decreasing  $f$  during haze formation, driving a large decrease in bulk-phase viscosity from  $> 10^8$  to  $< 10^2$  Pa s as proved by viscosity measurement, which may enhance the gas–particle mass transfer. ALW reduces the viscosity and triggers the phase transition, thus facilitating the uptake of precursors and oxidants and potentially altering the reaction pathway (Tillmann et al., 2010; Berkemeier et al., 2016; Li et al., 2018; Zhao et al., 2019).

For non-liquid particles, ALW facilitates the SOA formation via partition and heterogeneous uptake of water-soluble organics from gas phase into the particle phase, leading to a rapid increase in SOA along with ALW (Herrmann et al., 2015; Gkatzelis et al., 2021; Lim et al., 2010; El-Sayed et al., 2015). Subsequent aqueous-phase reactions may occur to form oligomers, organosulfates, and nitrogen-containing organics through radical or non-radical reactions (Surratt et al., 2007; Iinuma et al., 2007; Galloway et al., 2009; Lim et al., 2013; Y. Wang et al., 2020b). However, these reactions may be limited in non-liquid particles by the lower diffusivity due to higher viscosity. In contrast, liquid particles provide unstrained mass transfer of necessary oxidants and precursors between gas and particle phase, which is favorable for aqueous-phase processing. It is well known that aqueous-phase processing can contribute more oxidized SOA (Xu et al., 2017; Ervens et al., 2011; Zheng et al., 2023). Recent field studies have demonstrated that oligomers or dicar-



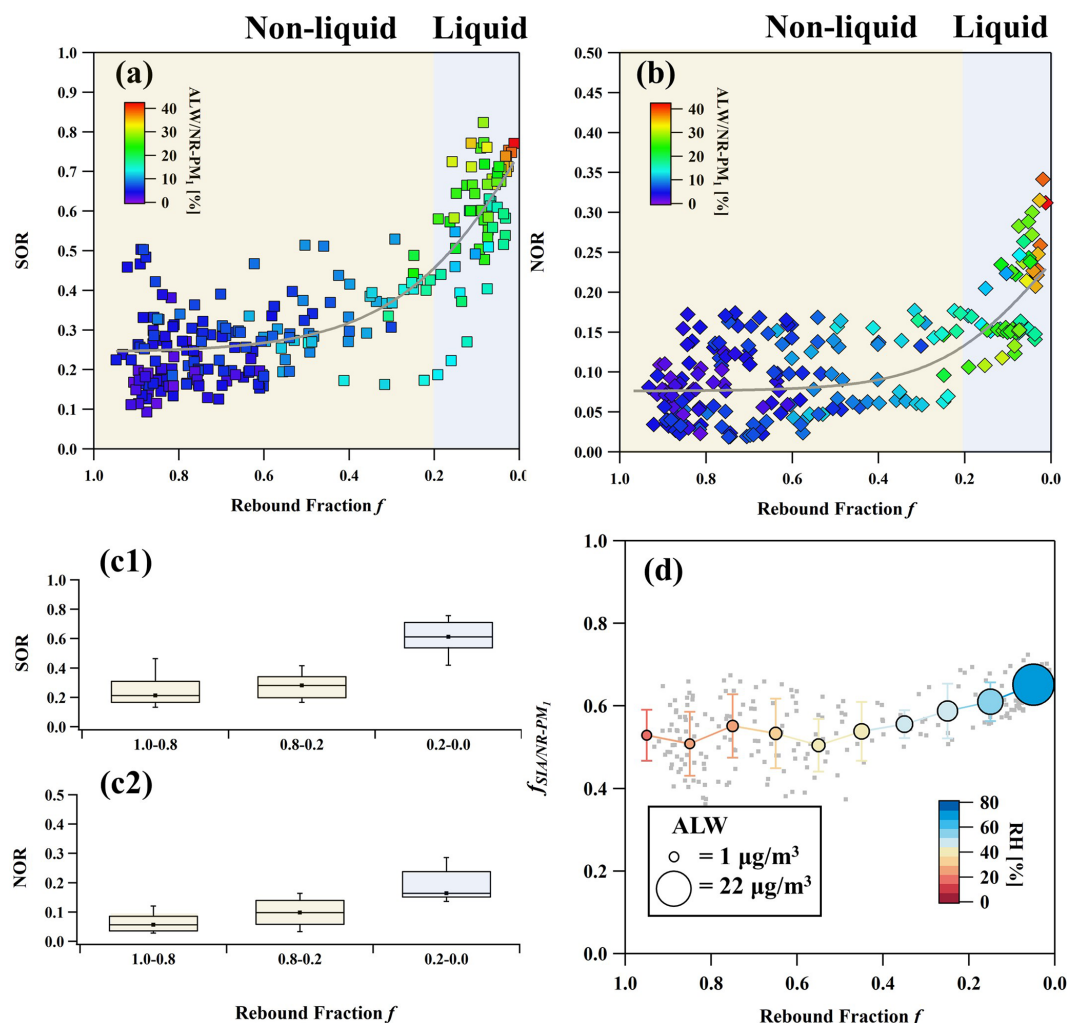


**Figure 4.** SOR and NOR as a function of  $f$  (a, b), relationship between SOR or NOR and three phase transition level (c1, c2), and the mass fraction of SIA in NR-PM<sub>1</sub> as a function of  $f$  during haze episodes (d). Non-liquid particles are marked by yellow shading, and liquid particles are marked by blue shading. In panels (a) and (b), the scatter points are colored by ALW / NR-PM<sub>1</sub>, and the trend lines are obtained by sigmoid fitting. In panels (c1) and (c2), the box plots show 10th, 25th, median, 75th, and 90th percentiles. In panel (d), RH is indicated by color, and ALW mass concentration is indicated by the size of the circle. The error bars show 1 standard deviation.

boxylic acids were enriched in liquid particles from the reactive uptake of methylglyoxal during the severe haze episodes in Beijing (Zheng et al., 2021). These oxidation products formed through aqueous-phase reactions are typically more oxidized and less volatile than those formed through gas-phase photochemistry (Ervens et al., 2011), which can be reserved in the particle phase and increase the SOA mass in total OA. Therefore, the significant growth of SOA / POA and  $f_{44}$  after phase transition is attributed by the enhanced heterogeneous or aqueous-phase reactions in liquid particles with abundant ALW during the nighttime.

### 3.5 Positive feedback loops between ALW and secondary aerosol formation triggered by phase transition during haze episodes

In Fig. 6a, the relationship between the overall particle hygroscopicity ( $k_{\text{total}}$ ) and RH is displayed. The  $k_{\text{total}}$ , ALW, and NR-PM<sub>1</sub> mass were grouped and averaged corresponding to an RH bin width of 10%. When RH was below 30%, the averaged  $k_{\text{total}}$  was  $\sim 0.35$ . However, it increased to 0.39 with higher ALW and NR-PM<sub>1</sub> mass at RH = 40%–60% and further rose to 0.43 with an average maximum NR-PM<sub>1</sub> value of  $56 \mu\text{g m}^{-3}$  when RH reached 70%–80%. This indicates that hygroscopic growth of particulate matter underwent two stages with increasing RH and NR-PM<sub>1</sub> mass, particularly at RH = 40%–60% and RH > 70%. From the above discussion, we have demonstrated that the non-liquid

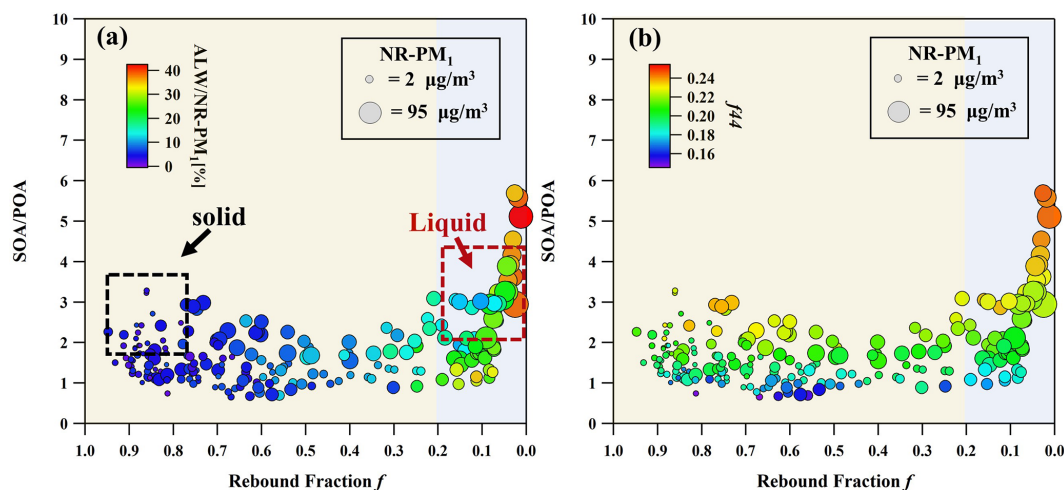


**Figure 5.** The relationship between SOA / POA and particle rebound fraction  $f$  for phase transition (a) and oxidation degree (b) during haze episodes. Non-liquid particles are marked by yellow shading, and liquid particles are marked by blue shading. The circles are colored by ALW / NR-PM<sub>1</sub> and  $f_{44}$  to represent water uptake capacity and particle oxidation degree in panels (a) and (b), respectively. The sizes of the circles are scaled to NR-PM<sub>1</sub> mass concentrations. The black (red) frame with the dashed line represents the offline viscosity measurement results using a poke-and-flow technique, corresponding to Fig. 1.

to liquid phase transition was triggered by the increased ALW, with a transition RH threshold of 40 %–60 % during haze episodes (as indicated by gradual color change in Fig. 6a). Phase transition facilitated the formation of sulfate and nitrate aerosols, contributing higher proportion of SIA in total particles under higher RH conditions. Notably, this led to a continuous increase in the volume fraction of inorganics with increasing RH (Fig. 6b). Besides,  $k_{\text{inorg}}$  also slightly increased when RH reached 60 % due to increased nitrate contribution in total SIA during haze episodes (Figs. 6c and S5). This may explain the first enhancement of  $k_{\text{total}}$  at RH = 40 %–60 %, which was mainly driven by the large increase in  $\text{frac}_{\text{inorg}}$  favored by phase transition.

Furthermore, the increase in  $k_{\text{total}}$ , coupled with elevated RH levels, led to a greater abundance of ALW mass. Heterogeneous or aqueous-phase reactions were favored with increasing ALW, promoting the formation of more oxidized SOA in liquid particles. At RH > 70 %, the significant increase in  $k_{\text{org}}$  (~ 14 %) compensated for the negative effect of decreased  $\text{frac}_{\text{org}}$  on the total hygroscopicity contributed by organics ( $k_{\text{org}} \cdot \text{frac}_{\text{org}}$ ), leading to a stable  $k_{\text{org}} \cdot \text{frac}_{\text{org}}$  with increasing RH (Figs. 6c and S15). This, in turn, coordinated with the increased  $\text{frac}_{\text{inorg}}$ , resulting in the second enhancement of  $k_{\text{total}}$ . As a result, phase transition accompanied by increasing ALW mass triggered a noticeable enhancement in  $k_{\text{total}}$ , with a mean value of 23 % during haze episodes. The enhanced water uptake ability of aerosols is expected to contribute more ALW under elevated RH conditions, further facilitating the secondary aerosol formation and deteriorating air quality. These results indicate that the establishment of positive feedback loops between ALW and

secondary aerosol formation was triggered by phase transition during haze episodes.

#### 4 Conclusion and atmospheric implications

Our findings revealed that particles predominantly exist in a semi-solid or solid state during clean winter days with RH below 30 %. However, a non-liquid to a liquid phase transition occurs when the ALW mass fraction surpassed 15 % (dry mass) at transition RH thresholds ranging from 40 % to 60 %. Additionally, we observed a consistent pattern in the non-liquid to liquid phase transition during haze formation, as manifested by both particle rebound fraction and bulk-phase viscosity measurements. Specifically, the decrease in  $f$  from > 0.8 to 0 corresponded to a viscosity transition ranging from  $\sim 10^8$  to  $\sim 10^2$  Pa s. With the incorporation of  $k_{\text{total}}$  into  $T_g$  calculation for ambient OA, we found that the characteristic of  $T_g/T$  versus ALW / NR-PM<sub>1</sub> agrees well with our field observations. This finding offers insights into the effectiveness of ALW / NR-PM<sub>1</sub> as an indicator for quantifying the moisture-induced phase transition capacity of atmospheric particles. Furthermore, incorporating overall particle hygroscopicity into the  $T_g$  calculation may potentially enhance OA viscosity simulations, especially in regions with a high proportion of inorganic salts under humid conditions. During haze episodes, SOR and NOR rapidly increased through phase transition and increased ALW by 48 % and 11 %, respectively, resulting in noticeable increases in SIA. The presence of abundant ALW, favored by elevated RH and higher proportion of SIA, facilitates heterogeneous and aqueous processes in liquid particles, leading to a substantial increase in the formation of secondary organic aerosols

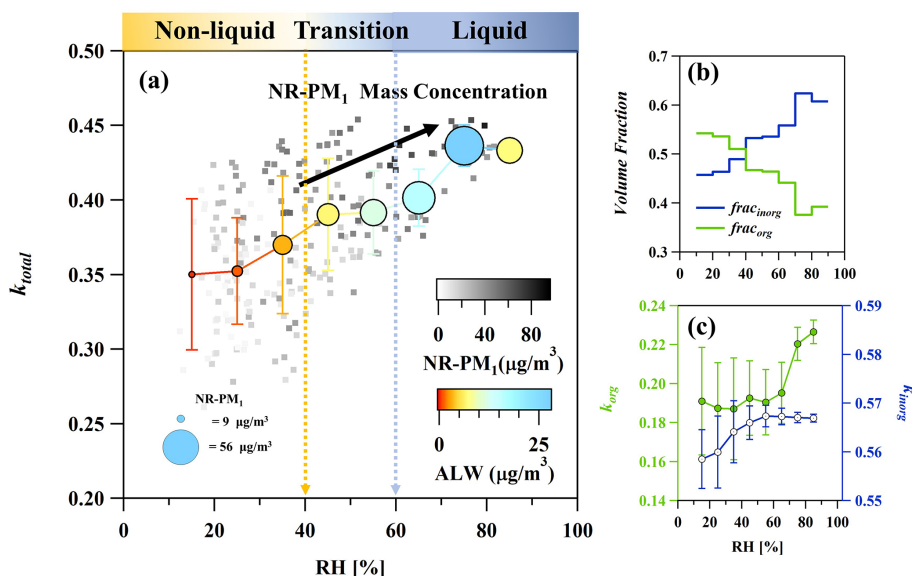


**Figure 6.** The overall hygroscopicity of particles (a), average volume fraction (b), and hygroscopicity (c) of inorganics and organics as a function of RH during haze episodes.  $k_{\text{total}}$  was calculated using real-time  $k_{\text{org}}$ . Particles in different phase state conditions, including non-liquid, the phase transition from non-liquid to liquid, and liquid, are visually distinguished through a gradual color change from yellow to blue, which correlates with RH. In panel (a), the scatter points are colored by NR-PM<sub>1</sub> mass concentrations and averaged in each RH bin. Averaged ALW and NR-PM<sub>1</sub> mass concentrations are indicated by color and size of the circle, respectively. The error bars show 1 standard deviation.

and elevated aerosol oxidation. As a result, the overall hygroscopicity parameters exhibit a substantial enhancement, with a mean value of 23 %.

In our previous studies, we have revealed the positive feedback loops between ALW and anthropogenic SIA at elevated RH levels during haze formation (Wu et al., 2018; Y. Wang et al., 2020a). The contribution of abundant ALW to SOA production has also been reported in various regions with active anthropogenic emissions, such as the Po Valley in Italy; the southeastern United States; and Beijing, China (Carlton and Turpin, 2013; Hodas et al., 2014; Xu et al., 2017). However, we observed that secondary transformation of SIA and SOA was significantly enhanced after phase transition with higher ALW mass during the observation. Our findings indicate that secondary aerosol formation could be impeded in non-liquid particles due to limited mass transfer between gas and particle phase for relevant reaction components (Ravisankara, 1997; Shiraiwa et al., 2011; Abbatt et al., 2012; Ma et al., 2022), whereas it is facilitated in liquid particles. It is therefore recommended that the non-liquid to liquid phase transition may be considered to be the kick-off for the positive feedback loops between ALW and secondary aerosol formation during haze events. This can be further supported by the case studies for varying polluted episodes, where episodes with phase transition generally exhibit a higher secondary transformation rate of secondary aerosols compared to episodes without phase transition (Sect. S7 and Fig. S16). This mechanism is expected to gain significance in other re-

gions with abundant anthropogenic emissions and high background RH during haze formation.

**Data availability.** The data presented in this article can be accessed from the corresponding author Zhijun Wu (zhijunwu@pku.edu.cn).

**Supplement.** The supplement related to this article is available online at: <https://doi.org/10.5194/acp-24-2399-2024-supplement>.

**Author contributions.** XM and ZW conceived the study. XM conducted the experiments; analyzed the experimental data; and wrote the manuscript with contributions from ZW, MS, JL, and MH. JC participated in the offline experiments and data analysis. YQ and TZ participated in the field experiments and conducted the filter sampling.

**Competing interests.** The contact author has declared that none of the authors has any competing interests.

**Disclaimer.** Publisher's note: Copernicus Publications remains neutral with regard to jurisdictional claims made in the text, published maps, institutional affiliations, or any other geographical representation in this paper. While Copernicus Publications makes ev-

ery effort to include appropriate place names, the final responsibility lies with the authors.

**Acknowledgements.** We sincerely thank our two referees for their valuable comments and constructive suggestions to improve the scientific rigor of our paper. We gratefully acknowledge the assistance of Wenfei Zhu for the technical support with Q-ACSM running and instrument calibration during the campaign.

**Financial support.** This research has been supported by the National Natural Science Foundation of China (grant no. 42375093) and the Fine Particle Research Initiative in East Asia Considering National Differences (FRIEND) project through the National Research Foundation of Korea (NRF: 2020M3G1A1114537), funded by the Ministry of Science and ICT, South Korea.

**Review statement.** This paper was edited by Dara Salcedo and reviewed by two anonymous referees.

## References

- Abbatt, J. P. D., Lee, A. K. Y., and Thornton, J. A.: Quantifying trace gas uptake to tropospheric aerosol: recent advances and remaining challenges, *Chem. Soc. Rev.*, 41, 6555–6581, 2012.
- Angell, C. A.: Relaxation in Liquids, Polymers and Plastic Crystals – Strong Fragile Patterns and Problems, *J. Non-Cryst. Solids*, 131, 13–31, 1991.
- Bateman, A. P., Belassein, H., and Martin, S. T.: Impactor Apparatus for the Study of Particle Rebound: Relative Humidity and Capillary Forces, *Aerosol Sci. Technol.*, 48, 42–52, <https://doi.org/10.1080/02786826.2013.853866>, 2014.
- Bateman, A. P., Gong, Z. H., Liu, P. F., Sato, B., Cirino, G., Zhang, Y., Artaxo, P., Bertram, A. K., Manzi, A. O., Rizzo, L. V., Souza, R. A. F., Zaveri, R. A., and Martin, S. T.: Sub-micrometre particulate matter is primarily in liquid form over Amazon rainforest, *Nat. Geosci.*, 9, 34–37, <https://doi.org/10.1038/Ngeo2599>, 2016.
- Bateman, A. P., Gong, Z., Harder, T. H., de Sá, S. S., Wang, B., Castillo, P., China, S., Liu, Y., O'Brien, R. E., Palm, B. B., Shiu, H.-W., Cirino, G. G., Thalman, R., Adachi, K., Alexander, M. L., Artaxo, P., Bertram, A. K., Buseck, P. R., Gilles, M. K., Jimenez, J. L., Laskin, A., Manzi, A. O., Sedlacek, A., Souza, R. A. F., Wang, J., Zaveri, R., and Martin, S. T.: Anthropogenic influences on the physical state of submicron particulate matter over a tropical forest, *Atmos. Chem. Phys.*, 17, 1759–1773, <https://doi.org/10.5194/acp-17-1759-2017>, 2017.
- Berkemeier, T., Steimer, S. S., Krieger, U. K., Peter, T., Pöschl, U., Ammann, M., and Shiraiwa, M.: Ozone uptake on glassy, semi-solid and liquid organic matter and the role of reactive oxygen intermediates in atmospheric aerosol chemistry, *Phys. Chem. Chem. Phys.*, 18, 12662–12674, <https://doi.org/10.1039/C6CP00634E>, 2016.
- Canagaratna, M. R., Jimenez, J. L., Kroll, J. H., Chen, Q., Kessler, S. H., Massoli, P., Hildebrandt Ruiz, L., Fortner, E., Williams, L. R., Wilson, K. R., Surratt, J. D., Donahue, N. M., Jayne, J. T., and Worsnop, D. R.: Elemental ratio measurements of organic compounds using aerosol mass spectrometry: characterization, improved calibration, and implications, *Atmos. Chem. Phys.*, 15, 253–272, <https://doi.org/10.5194/acp-15-253-2015>, 2015.
- Carlton, A. G. and Turpin, B. J.: Particle partitioning potential of organic compounds is highest in the Eastern US and driven by anthropogenic water, *Atmos. Chem. Phys.*, 13, 10203–10214, <https://doi.org/10.5194/acp-13-10203-2013>, 2013.
- Cerully, K. M., Bougiatioti, A., Hite Jr., J. R., Guo, H., Xu, L., Ng, N. L., Weber, R., and Nenes, A.: On the link between hygroscopicity, volatility, and oxidation state of ambient and water-soluble aerosols in the southeastern United States, *Atmos. Chem. Phys.*, 15, 8679–8694, <https://doi.org/10.5194/acp-15-8679-2015>, 2015.
- Chang, R. Y.-W., Slowik, J. G., Shantz, N. C., Vlasenko, A., Liggio, J., Sjostedt, S. J., Leaitch, W. R., and Abbatt, J. P. D.: The hygroscopicity parameter ( $\kappa$ ) of ambient organic aerosol at a field site subject to biogenic and anthropogenic influences: relationship to degree of aerosol oxidation, *Atmos. Chem. Phys.*, 10, 5047–5064, <https://doi.org/10.5194/acp-10-5047-2010>, 2010.
- Chen, Y., Wang, Y., Nenes, A., Wild, O., Song, S. J., Hu, D. W., Liu, D. T., He, J. J., Ruiz, L. H., Apte, J. S., Gunthe, S. S., and Liu, P. F.: Ammonium Chloride Associated Aerosol Liquid Water Enhances Haze in Delhi, India, *Environ. Sci. Technol.*, 56, 7163–7173, <https://doi.org/10.1021/acs.est.2c00650>, 2022.
- Cheng, Y., Zheng, G., Wei, C., Mu, Q., Zheng, B., Wang, Z., Gao, M., Zhang, Q., He, K., Carmichael, G., Pöschl, U., and Su, H.: Reactive nitrogen chemistry in aerosol water as a source of sulfate during haze events in China, *Sci. Adv.*, 2, e1601530, <https://doi.org/10.1126/sciadv.1601530>, 2016.
- Ciobanu, V. G., Marcolli, C., Krieger, U. K., Weers, U., and Peter, T.: Liquid-Liquid Phase Separation in Mixed Organic/Inorganic Aerosol Particles, *J. Phys. Chem. A*, 113, 10966–10978, 2009.
- DeRieux, W.-S. W., Li, Y., Lin, P., Laskin, J., Laskin, A., Bertram, A. K., Nizkorodov, S. A., and Shiraiwa, M.: Predicting the glass transition temperature and viscosity of secondary organic material using molecular composition, *Atmos. Chem. Phys.*, 18, 6331–6351, <https://doi.org/10.5194/acp-18-6331-2018>, 2018.
- Dette, H. P., Qi, M., Schröder, D. C., Godt, A., and Koop, T.: Glass-Forming Properties of 3-Methylbutane-1,2,3-tricarboxylic Acid and Its Mixtures with Water and Pinonic Acid, *J. Phys. Chem. A*, 118, 7024–7033, <https://doi.org/10.1021/jp505910w>, 2014.
- Duplissy, J., DeCarlo, P. F., Dommen, J., Alfarra, M. R., Metzger, A., Barmapadimos, I., Prevot, A. S. H., Weingartner, E., Tritscher, T., Gysel, M., Aiken, A. C., Jimenez, J. L., Canagaratna, M. R., Worsnop, D. R., Collins, D. R., Tomlinson, J., and Baltensperger, U.: Relating hygroscopicity and composition of organic aerosol particulate matter, *Atmos. Chem. Phys.*, 11, 1155–1165, <https://doi.org/10.5194/acp-11-1155-2011>, 2011.
- El-Sayed, M. M. H., Wang, Y. Q., and Hennigan, C. J.: Direct atmospheric evidence for the irreversible formation of aqueous secondary organic aerosol, *Geophys. Res. Lett.*, 42, 5577–5586, <https://doi.org/10.1002/2015gl064556>, 2015.
- Ervens, B., Turpin, B. J., and Weber, R. J.: Secondary organic aerosol formation in cloud droplets and aqueous particles (aq-SOA): a review of laboratory, field and model studies, *Atmos. Chem. Phys.*, 11, 11069–11102, <https://doi.org/10.5194/acp-11-11069-2011>, 2011.
- Fountoukis, C. and Nenes, A.: ISORROPIA II: a computationally efficient thermodynamic equilibrium model for  $K^+$ -

- $\text{Ca}^{2+}$ – $\text{Mg}^{2+}$ – $\text{NH}_4^+$ – $\text{Na}^+$ – $\text{SO}_4^{2-}$ – $\text{NO}_3^-$ – $\text{Cl}^-$ – $\text{H}_2\text{O}$  aerosols, *Atmos. Chem. Phys.*, 7, 4639–4659, <https://doi.org/10.5194/acp-7-4639-2007>, 2007.
- Galloway, M. M., Chhabra, P. S., Chan, A. W. H., Surratt, J. D., Flagan, R. C., Seinfeld, J. H., and Keutsch, F. N.: Glyoxal uptake on ammonium sulphate seed aerosol: reaction products and reversibility of uptake under dark and irradiated conditions, *Atmos. Chem. Phys.*, 9, 3331–3345, <https://doi.org/10.5194/acp-9-3331-2009>, 2009.
- Gkatzelis, G. I., Papanastasiou, D. K., Karydis, V. A., Hohaus, T., Liu, Y., Schmitt, S. H., Schlag, P., Fuchs, H., Novelli, A., Chen, Q., Cheng, X., Broch, S., Dong, H., Holland, F., Li, X., Liu, Y. H., Ma, X. F., Reimer, D., Rohrer, F., Shao, M., Tan, Z., Taraborrelli, D., Tillmann, R., Wang, H. C., Wang, Y., Wu, Y. S., Wu, Z. J., Zeng, L. M., Zheng, J., Hu, M., Lu, K. D., Hofzumahaus, A., Zhang, Y. H., Wahner, A., and Kiendler-Scharr, A.: Uptake of Water-soluble Gas-phase Oxidation Products Drives Organic Particulate Pollution in Beijing, *Geophys. Res. Lett.*, 48, e2020GL091351, <https://doi.org/10.1029/2020GL091351>, 2021.
- Gunthe, S. S., Rose, D., Su, H., Garland, R. M., Achtert, P., Nowak, A., Wiedensohler, A., Kuwata, M., Takegawa, N., Kondo, Y., Hu, M., Shao, M., Zhu, T., Andreae, M. O., and Pöschl, U.: Cloud condensation nuclei (CCN) from fresh and aged air pollution in the megacity region of Beijing, *Atmos. Chem. Phys.*, 11, 11023–11039, <https://doi.org/10.5194/acp-11-11023-2011>, 2011.
- Guo, H., Xu, L., Bougiatioti, A., Cerully, K. M., Capps, S. L., Hite Jr., J. R., Carlton, A. G., Lee, S.-H., Bergin, M. H., Ng, N. L., Nenes, A., and Weber, R. J.: Fine-particle water and pH in the southeastern United States, *Atmos. Chem. Phys.*, 15, 5211–5228, <https://doi.org/10.5194/acp-15-5211-2015>, 2015.
- Gysel, M., Crosier, J., Topping, D. O., Whitehead, J. D., Bower, K. N., Cubison, M. J., Williams, P. I., Flynn, M. J., McFiggans, G. B., and Coe, H.: Closure study between chemical composition and hygroscopic growth of aerosol particles during TORCH2, *Atmos. Chem. Phys.*, 7, 6131–6144, <https://doi.org/10.5194/acp-7-6131-2007>, 2007.
- Herrmann, H., Schaefer, T., Tilgner, A., Styler, S. A., Weller, C., Teich, M., and Otto, T.: Tropospheric Aqueous-Phase Chemistry: Kinetics, Mechanisms, and Its Coupling to a Changing Gas Phase, *Chem. Rev.*, 115, 4259–4334, <https://doi.org/10.1021/cr500447k>, 2015.
- Hodas, N., Sullivan, A. P., Skog, K., Keutsch, F. N., Collett, J. L., Decesari, S., Facchini, M. C., Carlton, A. G., Laaksonen, A., and Turpin, B. J.: Aerosol Liquid Water Driven by Anthropogenic Nitrate: Implications for Lifetimes of Water-Soluble Organic Gases and Potential for Secondary Organic Aerosol Formation, *Environ. Sci. Technol.*, 48, 11127–11136, 2014.
- Hodas, N., Zuend, A., Mui, W., Flagan, R. C., and Seinfeld, J. H.: Influence of particle-phase state on the hygroscopic behavior of mixed organic–inorganic aerosols, *Atmos. Chem. Phys.*, 15, 5027–5045, <https://doi.org/10.5194/acp-15-5027-2015>, 2015.
- Hu, S. Y., Zhao, G., Tan, T. Y., Li, C. C., Zong, T. M., Xu, N., Zhu, W. F., and Hu, M.: Current challenges of improving visibility due to increasing nitrate fraction in  $\text{PM}_{2.5}$  during the haze days in Beijing, China, *Environ. Pollut.*, 290, 118032, <https://doi.org/10.1016/j.envpol.2021.118032>, 2021.
- Iinuma, Y., Muller, C., Berndt, T., Boge, O., Claeys, M., and Herrmann, H.: Evidence for the existence of organosulfates from beta-pinene ozonolysis in ambient secondary organic aerosol, *Environ. Sci. Technol.*, 41, 6678–6683, <https://doi.org/10.1021/es070938t>, 2007.
- Jia, L., Xu, Y., and Duan, M.: Explosive formation of secondary organic aerosol due to aerosol-fog interactions, *Sci. Total Environ.*, 866, 161338, <https://doi.org/10.1016/j.scitotenv.2022.161338>, 2023.
- Jin, X., Wang, Y., Li, Z., Zhang, F., Xu, W., Sun, Y., Fan, X., Chen, G., Wu, H., Ren, J., Wang, Q., and Cribb, M.: Significant contribution of organics to aerosol liquid water content in winter in Beijing, China, *Atmos. Chem. Phys.*, 20, 901–914, <https://doi.org/10.5194/acp-20-901-2020>, 2020.
- Knopf, D. A. and Alpert, P. A.: Atmospheric ice nucleation, *Nat. Rev. Phys.*, 5, 203–217, <https://doi.org/10.1038/s42254-023-00570-7>, 2023.
- Koop, T., Bookhold, J., Shiraiwa, M., and Pöschl, U.: Glass transition and phase state of organic compounds: dependency on molecular properties and implications for secondary organic aerosols in the atmosphere, *Phys. Chem. Chem. Phys.*, 13, 19238–19255, <https://doi.org/10.1039/c1cp22617g>, 2011.
- Kuang, Y., He, Y., Xu, W., Zhao, P., Cheng, Y., Zhao, G., Tao, J., Ma, N., Su, H., Zhang, Y., Sun, J., Cheng, P., Yang, W., Zhang, S., Wu, C., Sun, Y., and Zhao, C.: Distinct diurnal variation in organic aerosol hygroscopicity and its relationship with oxygenated organic aerosol, *Atmos. Chem. Phys.*, 20, 865–880, <https://doi.org/10.5194/acp-20-865-2020>, 2020.
- Lei, L., Zhou, W., Chen, C., He, Y., Li, Z. J., Sun, J. X., Tang, X., Fu, P. Q., Wang, Z. F., and Sun, Y. L.: Long-term characterization of aerosol chemistry in cold season from 2013 to 2020 in Beijing, China, *Environ. Pollut.*, 268, 115952, <https://doi.org/10.1016/j.envpol.2020.115952>, 2021.
- Lelieveld, J., Evans, J. S., Fnais, M., Giannadaki, D., and Pozzer, A.: The contribution of outdoor air pollution sources to premature mortality on a global scale, *Nature*, 525, 367–371, <https://doi.org/10.1038/nature15371>, 2015.
- Li, X., Song, S., Zhou, W., Hao, J., Worsnop, D. R., and Jiang, J.: Interactions between aerosol organic components and liquid water content during haze episodes in Beijing, *Atmos. Chem. Phys.*, 19, 12163–12174, <https://doi.org/10.5194/acp-19-12163-2019>, 2019.
- Li, Y. and Shiraiwa, M.: Timescales of secondary organic aerosols to reach equilibrium at various temperatures and relative humidities, *Atmos. Chem. Phys.*, 19, 5959–5971, <https://doi.org/10.5194/acp-19-5959-2019>, 2019.
- Li, Y. J., Sun, Y., Zhang, Q., Li, X., Li, M., Zhou, Z., and Chan, C. K.: Real-time chemical characterization of atmospheric particulate matter in China: A review, *Atmos. Environ.*, 158, 270–304, <https://doi.org/10.1016/j.atmosenv.2017.02.027>, 2017.
- Li, Z., Smith, K. A., and Cappa, C. D.: Influence of relative humidity on the heterogeneous oxidation of secondary organic aerosol, *Atmos. Chem. Phys.*, 18, 14585–14608, <https://doi.org/10.5194/acp-18-14585-2018>, 2018.
- Lim, Y. B., Tan, Y., Perri, M. J., Seitzinger, S. P., and Turpin, B. J.: Aqueous chemistry and its role in secondary organic aerosol (SOA) formation, *Atmos. Chem. Phys.*, 10, 10521–10539, <https://doi.org/10.5194/acp-10-10521-2010>, 2010.
- Lim, Y. B., Tan, Y., and Turpin, B. J.: Chemical insights, explicit chemistry, and yields of secondary organic aerosol from OH radical oxidation of methylglyoxal and glyoxal in

- the aqueous phase, *Atmos. Chem. Phys.*, 13, 8651–8667, <https://doi.org/10.5194/acp-13-8651-2013>, 2013.
- Liu, P., Song, M., Zhao, T., Gunthe, S. S., Ham, S., He, Y., Qin, Y. M., Gong, Z., Amorim, J. C., Bertram, A. K., and Martin, S. T.: Resolving the mechanisms of hygroscopic growth and cloud condensation nuclei activity for organic particulate matter, *Nat. Commun.*, 9, 4076, <https://doi.org/10.1038/s41467-018-06622-2>, 2018.
- Liu, T., Clegg, S. L., and Abbatt, J. P. D.: Fast oxidation of sulfur dioxide by hydrogen peroxide in deliquesced aerosol particles, *P. Natl. Acad. Sci. USA*, 117, 1354–1359, <https://doi.org/10.1073/pnas.1916401117>, 2020.
- Liu, Y., Wu, Z., Wang, Y., Xiao, Y., Gu, F., Zheng, J., Tan, T., Shang, D., Wu, Y., Zeng, L., Hu, M., Bateman, A. P., and Martin, S. T.: Submicrometer Particles Are in the Liquid State during Heavy Haze Episodes in the Urban Atmosphere of Beijing, China, *Environ. Sci. Technol. Lett.*, 4, 427–432, <https://doi.org/10.1021/acs.estlett.7b00352>, 2017.
- Liu, Y., Wu, Z., Huang, X., Shen, H., Bai, Y., Qiao, K., Meng, X., Hu, W., Tang, M., and He, L.: Aerosol Phase State and Its Link to Chemical Composition and Liquid Water Content in a Subtropical Coastal Megacity, *Environ. Sci. Technol.*, 53, 5027–5033, <https://doi.org/10.1021/acs.est.9b01196>, 2019.
- Liu, Y. C., Meng, X. X., Wu, Z. J., Huang, D. D., Wang, H. L., Chen, J., Chen, J. C., Zong, T. M., Fang, X., Tan, T. Y., Zhao, G., Chen, S. Y., Zeng, L. W., Guo, S., Huang, X. F., He, L. Y., Zeng, L. M., and Hu, M.: The particle phase state during the biomass burning events, *Sci. Total Environ.*, 792, 148035, <https://doi.org/10.1016/j.scitotenv.2021.148035>, 2021.
- Ma, W., Zheng, F. X., Zhang, Y. S., Chen, X., Zhan, J. L., Hua, C. J., Song, B. Y., Wang, Z. C., Xie, J. L., Yan, C., Kulmala, M., and Liu, Y. C.: Weakened Gas-to-Particle Partitioning of Oxygenated Organic Molecules in Liquified Aerosol Particles, *Environ. Sci. Technol. Lett.*, 9, 837–843, <https://doi.org/10.1021/acs.estlett.2c00556>, 2022.
- Marshall, F. H., Berkemeier, T., Shiraiwa, M., Nandy, L., Ohm, P. B., Dutcher, C. S., and Reid, J. P.: Influence of particle viscosity on mass transfer and heterogeneous ozonolysis kinetics in aqueous-sucrose-maleic acid aerosol, *Phys. Chem. Chem. Phys.*, 20, 15560–15573, 2018.
- Matthew, B. M., Middlebrook, A. M., and Onasch, T. B.: Collection efficiencies in an Aerodyne Aerosol Mass Spectrometer as a function of particle phase for laboratory generated aerosols, *Aerosol Sci. Technol.*, 42, 884–898, <https://doi.org/10.1080/02786820802356797>, 2008.
- Meng, X. X. Y., Wu, Z. J., Guo, S., Wang, H., Liu, K. F., Zong, T. M., Liu, Y. C., Zhang, W. B., Zhang, Z., Chen, S. Y., Zeng, L. M., Hallquist, M., Shuai, S. J., and Hu, M.: Humidity-Dependent Phase State of Gasoline Vehicle Emission-Related Aerosols, *Environ. Sci. Technol.*, 55, 832–841, 2021.
- Mikhailov, E., Vlasenko, S., Martin, S. T., Koop, T., and Pöschl, U.: Amorphous and crystalline aerosol particles interacting with water vapor: conceptual framework and experimental evidence for restructuring, phase transitions and kinetic limitations, *Atmos. Chem. Phys.*, 9, 9491–9522, <https://doi.org/10.5194/acp-9-9491-2009>, 2009.
- Mu, Q., Shiraiwa, M., Octaviani, M., Ma, N., Ding, A. J., Su, H., Lammel, G., Pöschl, U., and Cheng, Y. F.: Temperature effect on phase state and reactivity controls atmospheric multi-phase chemistry and transport of PAHs, *Sci. Adv.*, 4, eaap7314, <https://doi.org/10.1126/sciadv.aap7314>, 2018.
- Murray, B. J., Wilson, T. W., Dobbie, S., Cui, Z. Q., Al-Jumur, S. M. R. K., Mohler, O., Schnaiter, M., Wagner, R., Benz, S., Niemand, M., Saathoff, H., Ebert, V., Wagner, S., and Karcher, B.: Heterogeneous nucleation of ice particles on glassy aerosols under cirrus conditions, *Nat. Geosci.*, 3, 233–237, 2010.
- Ng, N. L., Canagaratna, M. R., Zhang, Q., Jimenez, J. L., Tian, J., Ulbrich, I. M., Kroll, J. H., Docherty, K. S., Chhabra, P. S., Bahreini, R., Murphy, S. M., Seinfeld, J. H., Hildebrandt, L., Donahue, N. M., DeCarlo, P. F., Lanz, V. A., Prévôt, A. S. H., Dinar, E., Rudich, Y., and Worsnop, D. R.: Organic aerosol components observed in Northern Hemispheric datasets from Aerosol Mass Spectrometry, *Atmos. Chem. Phys.*, 10, 4625–4641, <https://doi.org/10.5194/acp-10-4625-2010>, 2010.
- Ng, N. L., Herndon, S. C., Trimborn, A., Canagaratna, M. R., Croteau, P. L., Onasch, T. B., Sueper, D., Worsnop, D. R., Zhang, Q., Sun, Y. L., and Jayne, J. T.: An Aerosol Chemical Speciation Monitor (ACSM) for Routine Monitoring of the Composition and Mass Concentrations of Ambient Aerosol, *Aerosol Sci. Technol.*, 45, 780–794, <https://doi.org/10.1080/02786826.2011.560211>, 2011.
- Nguyen, T. K. V., Zhang, Q., Jimenez, J. L., Pike, M., and Carlton, A. G.: Liquid Water: Ubiquitous Contributor to Aerosol Mass, *Environ. Sci. Technol. Lett.*, 3, 257–263, 2016.
- Pajunoja, A., Hu, W., Leong, Y. J., Taylor, N. F., Miettinen, P., Palm, B. B., Mikkonen, S., Collins, D. R., Jimenez, J. L., and Virtanen, A.: Phase state of ambient aerosol linked with water uptake and chemical aging in the southeastern US, *Atmos. Chem. Phys.*, 16, 11163–11176, <https://doi.org/10.5194/acp-16-11163-2016>, 2016.
- Peckhaus, A., Grass, S., Treuel, L., and Zellner, R.: Deliquescence and Efflorescence Behavior of Ternary Inorganic/Organic/Water Aerosol Particles, *J. Phys. Chem. A*, 116, 6199–6210, <https://doi.org/10.1021/jp211522t>, 2012.
- Peng, C., Chen, L. X. D., and Tang, M. J.: A database for deliquescence and efflorescence relative humidities of compounds with atmospheric relevance, *Fund. Res.-China*, 2, 578–587, <https://doi.org/10.1016/j.fmre.2021.11.021>, 2022.
- Petters, M. D. and Kreidenweis, S. M.: A single parameter representation of hygroscopic growth and cloud condensation nucleus activity, *Atmos. Chem. Phys.*, 7, 1961–1971, <https://doi.org/10.5194/acp-7-1961-2007>, 2007.
- Petters, S. S., Kreidenweis, S. M., Grieshop, A. P., Ziemann, P. J., and Petters, M. D.: Temperature- and Humidity-Dependent Phase States of Secondary Organic Aerosols, *Geophys. Res. Lett.*, 46, 1005–1013, <https://doi.org/10.1029/2018GL080563>, 2019.
- Pöschl, U.: Atmospheric Aerosols: Composition, Transformation, Climate and Health Effects, *Angew. Chem. Int. Edit.*, 44, 7520–7540, <https://doi.org/10.1002/anie.200501122>, 2005.
- Ravishankara, A. R.: Heterogeneous and multiphase chemistry in the troposphere, *Science*, 276, 1058–1065, 1997.
- Rothfuss, N. E. and Petters, M. D.: Influence of Functional Groups on the Viscosity of Organic Aerosol, *Environ. Sci. Technol.*, 51, 271–279, <https://doi.org/10.1021/acs.est.6b04478>, 2017.
- Saukko, E., Lambe, A. T., Massoli, P., Koop, T., Wright, J. P., Croasdale, D. R., Pedernera, D. A., Onasch, T. B., Laaksonen, A., Davidovits, P., Worsnop, D. R., and Virtanen, A.: Humidity-

- dependent phase state of SOA particles from biogenic and anthropogenic precursors, *Atmos. Chem. Phys.*, 12, 7517–7529, <https://doi.org/10.5194/acp-12-7517-2012>, 2012.
- Seinfeld, J. H. and Pandis, S. N.: *Atmospheric Chemistry and Physics: From Air Pollution to Climate Change*, Wiley, ISBN 978-0471720188, 2006.
- Seinfeld, J. H., Bretherton, C., Carslaw, K. S., Coe, H., DeMott, P. J., Dunlea, E. J., Feingold, G., Ghan, S., Guenther, A. B., Kahn, R., Kraucunas, I., Kreidenweis, S. M., Molina, M. J., Nenes, A., Penner, J. E., Prather, K. A., Ramanathan, V., Ramaswamy, V., Rasch, P. J., Ravishankara, A. R., Rosenfeld, D., Stephens, G., and Wood, R.: Improving our fundamental understanding of the role of aerosol-cloud interactions in the climate system, *P. Natl. Acad. Sci. USA*, 113, 5781–5790, <https://doi.org/10.1073/pnas.1514043113>, 2016.
- Shen, H., Chen, Z., Li, H., Qian, X., Qin, X., and Shi, W.: Gas-Particle Partitioning of Carbonyl Compounds in the Ambient Atmosphere, *Environ. Sci. Technol.*, 52, 10997–11006, <https://doi.org/10.1021/acs.est.8b01882>, 2018.
- Shiraiwa, M., Ammann, M., Koop, T., and Pöschl, U.: Gas uptake and chemical aging of semisolid organic aerosol particles, *P. Natl. Acad. Sci. USA*, 108, 11003–11008, <https://doi.org/10.1073/pnas.1103045108>, 2011.
- Shiraiwa, M., Zuend, A., Bertram, A. K., and Seinfeld, J. H.: Gas-particle partitioning of atmospheric aerosols: interplay of physical state, non-ideal mixing and morphology, *Phys. Chem. Chem. Phys.*, 15, 11441–11453, 2013.
- Shiraiwa, M., Li, Y., Tsimpidi, A. P., Karydis, V. A., Berke-meier, T., Pandis, S. N., Lelieveld, J., Koop, T., and Pöschl, U.: Global distribution of particle phase state in atmospheric secondary organic aerosols, *Nat. Commun.*, 8, 15002, <https://doi.org/10.1038/ncomms15002>, 2017.
- Song, M., Jeong, R., Kim, D., Qiu, Y., Meng, X., Wu, Z., Zuend, A., Ha, Y., Kim, C., Kim, H., Gaikwad, S., Jang, K.-S., Lee, J. Y., and Ahn, J.: Comparison of Phase States of PM<sub>2.5</sub> over Megacities, Seoul and Beijing, and Their Implications on Particle Size Distribution, *Environ. Sci. Technol.*, 56, 17581–17590, <https://doi.org/10.1021/acs.est.2c06377>, 2022.
- Song, M. J., Marcolli, C., Krieger, U. K., Lienhard, D. M., and Peter, T.: Morphologies of mixed organic/inorganic/aqueous aerosol droplets, *Faraday Discuss.*, 165, 289–316, 2013.
- Sun, Y. L., Wang, Z. F., Fu, P. Q., Yang, T., Jiang, Q., Dong, H. B., Li, J., and Jia, J. J.: Aerosol composition, sources and processes during wintertime in Beijing, China, *Atmos. Chem. Phys.*, 13, 4577–4592, <https://doi.org/10.5194/acp-13-4577-2013>, 2013.
- Sun, Y., Du, W., Wang, Q., Zhang, Q., Chen, C., Chen, Y., Chen, Z., Fu, P., Wang, Z., Gao, Z., and Worsnop, D. R.: Real-Time Characterization of Aerosol Particle Composition above the Urban Canopy in Beijing: Insights into the Interactions between the Atmospheric Boundary Layer and Aerosol Chemistry, *Environ. Sci. Technol.*, 49, 11340–11347, <https://doi.org/10.1021/acs.est.5b02373>, 2015.
- Surratt, J. D., Kroll, J. H., Kleindienst, T. E., Edney, E. O., Claeys, M., Sorooshian, A., Ng, N. L., Offenberg, J. H., Lewandowski, M., Jaoui, M., Flagan, R. C., and Seinfeld, J. H.: Evidence for organosulfates in secondary organic aerosol, *Environ. Sci. Technol.*, 41, 517–527, <https://doi.org/10.1021/es062081q>, 2007.
- Tang, M. J., Cox, R. A., and Kalberer, M.: Compilation and evaluation of gas phase diffusion coefficients of reactive trace gases in the atmosphere: volume 1. Inorganic compounds, *Atmos. Chem. Phys.*, 14, 9233–9247, <https://doi.org/10.5194/acp-14-9233-2014>, 2014.
- Tillmann, R., Hallquist, M., Jonsson, Å. M., Kiendler-Scharr, A., Saathoff, H., Iinuma, Y., and Mentel, Th. F.: Influence of relative humidity and temperature on the production of pinonaldehyde and OH radicals from the ozonolysis of  $\alpha$ -pinene, *Atmos. Chem. Phys.*, 10, 7057–7072, <https://doi.org/10.5194/acp-10-7057-2010>, 2010.
- Ushijima, S. B., Huynh, E., Davis, R. D., and Tolbert, M. A.: Seeded Crystal Growth of Internally Mixed Organic-Inorganic Aerosols: Impact of Organic Phase State, *J. Phys. Chem. A*, 125, 8668–8679, <https://doi.org/10.1021/acs.jpca.1c04471>, 2021.
- Wang, H., Chen, X., Lu, K., Tan, Z., Ma, X., Wu, Z., Li, X., Liu, Y., Shang, D., Wu, Y., Zeng, L., Hu, M., Schmitt, S., Kiendler-Scharr, A., Wahner, A., and Zhang, Y.: Wintertime N<sub>2</sub>O<sub>5</sub> uptake coefficients over the North China Plain, *Sci. Bull.*, 65, 765–774, <https://doi.org/10.1016/j.scib.2020.02.006>, 2020.
- Wang, J. F., Ye, J. H., Zhang, Q., Zhao, J., Wu, Y. Z., Li, J. Y., Liu, D. T., Li, W. J., Zhang, Y. G., Wu, C., Xie, C. H., Qin, Y. M., Lei, Y. L., Huang, X. P., Guo, J. P., Liu, P. F., Fu, P. Q., Li, Y. J., Lee, H. C., Choi, H., Zhang, J., Liao, H., Chen, M. D., Sun, Y. L., Ge, X. L., Martin, S. T., and Jacob, D. J.: Aqueous production of secondary organic aerosol from fossil-fuel emissions in winter Beijing haze, *P. Natl. Acad. Sci. USA*, 118, e2022179118, <https://doi.org/10.1073/pnas.2022179118>, 2021.
- Wang, Y., Chen, Y., Wu, Z., Shang, D., Bian, Y., Du, Z., Schmitt, S. H., Su, R., Gkatzelis, G. I., Schlag, P., Hohaus, T., Voliotis, A., Lu, K., Zeng, L., Zhao, C., Alfarra, M. R., McFiggans, G., Wiedensohler, A., Kiendler-Scharr, A., Zhang, Y., and Hu, M.: Mutual promotion between aerosol particle liquid water and particulate nitrate enhancement leads to severe nitrate-dominated particulate matter pollution and low visibility, *Atmos. Chem. Phys.*, 20, 2161–2175, <https://doi.org/10.5194/acp-20-2161-2020>, 2020a.
- Wang, Y., Hu, M., Wang, Y.-C., Li, X., Fang, X., Tang, R., Lu, S., Wu, Y., Guo, S., Wu, Z., Hallquist, M., and Yu, J. Z.: Comparative Study of Particulate Organosulfates in Contrasting Atmospheric Environments: Field Evidence for the Significant Influence of Anthropogenic Sulfate and NO<sub>x</sub>, *Environ. Sci. Technol. Lett.*, 7, 787–794, <https://doi.org/10.1021/acs.estlett.0c00550>, 2020b.
- Wang, Y., Li, Z., Wang, Q., Jin, X., Yan, P., Cribb, M., Li, Y., Yuan, C., Wu, H., Wu, T., Ren, R., and Cai, Z.: Enhancement of secondary aerosol formation by reduced anthropogenic emissions during Spring Festival 2019 and enlightenment for regional PM<sub>2.5</sub> control in Beijing, *Atmos. Chem. Phys.*, 21, 915–926, <https://doi.org/10.5194/acp-21-915-2021>, 2021.
- Williams, B. J., Goldstein, A. H., Kreisberg, N. M., and Hering, S. V.: In situ measurements of gas/particle-phase transitions for atmospheric semivolatile organic compounds, *P. Natl. Acad. Sci. USA*, 107, 6676–6681, <https://doi.org/10.1073/pnas.0911858107>, 2010.
- Wu, Z. J., Zheng, J., Shang, D. J., Du, Z. F., Wu, Y. S., Zeng, L. M., Wiedensohler, A., and Hu, M.: Particle hygroscopicity and its link to chemical composition in the urban atmosphere of Beijing, China, during summertime, *Atmos. Chem. Phys.*, 16, 1123–1138, <https://doi.org/10.5194/acp-16-1123-2016>, 2016.

- Wu, Z. J., Wang, Y., Tan, T. Y., Zhu, Y. S., Li, M. R., Shang, D. J., Wang, H. C., Lu, K. D., Guo, S., Zeng, L. M., and Zhang, Y. H.: Aerosol Liquid Water Driven by Anthropogenic Inorganic Salts: Implying Its Key Role in Haze Formation over the North China Plain, *Environ. Sci. Technol. Lett.*, 5, 160–166, 2018.
- Xu, W. Q., Han, T. T., Du, W., Wang, Q. Q., Chen, C., Zhao, J., Zhang, Y. J., Li, J., Fu, P. Q., Wang, Z. F., Worsnop, D. R., and Sun, Y. L.: Effects of Aqueous-Phase and Photochemical Processing on Secondary Organic Aerosol Formation and Evolution in Beijing, China, *Environ. Sci. Technol.*, 51, 762–770, <https://doi.org/10.1021/acs.est.6b04498>, 2017.
- Zhang, Q., Jimenez, J. L., Canagaratna, M. R., Ulbrich, I. M., Ng, N. L., Worsnop, D. R., and Sun, Y.: Understanding atmospheric organic aerosols via factor analysis of aerosol mass spectrometry: a review, *Anal. Bioanal. Chem.*, 401, 3045–3067, <https://doi.org/10.1007/s00216-011-5355-y>, 2011.
- Zhang, Y., Tang, L., Croteau, P. L., Favez, O., Sun, Y., Canagaratna, M. R., Wang, Z., Couvidat, F., Albinet, A., Zhang, H., Sciare, J., Prévôt, A. S. H., Jayne, J. T., and Worsnop, D. R.: Field characterization of the PM<sub>2.5</sub> Aerosol Chemical Speciation Monitor: insights into the composition, sources, and processes of fine particles in eastern China, *Atmos. Chem. Phys.*, 17, 14501–14517, <https://doi.org/10.5194/acp-17-14501-2017>, 2017.
- Zhang, Y., Chen, Y. Z., Lambe, A. T., Olson, N. E., Lei, Z. Y., Craig, R. L., Zhang, Z. F., Gold, A., Onasch, T. B., Jayne, J. T., Worsnop, D. R., Gaston, C. J., Thornton, J. A., Vizuete, W., Ault, A. P., and Surratt, J. D.: Effect of the Aerosol-Phase State on Secondary Organic Aerosol Formation from the Reactive Uptake of Isoprene-Derived Epoxydiols (IEPDX), *Environ. Sci. Technol. Lett.*, 5, 167–174, 2018.
- Zhao, Z., Xu, Q., Yang, X., and Zhang, H.: Heterogeneous Ozonolysis of Endocyclic Unsaturated Organic Aerosol Proxies: Implications for Criegee Intermediate Dynamics and Later-Generation Reactions, *ACS Earth Space Chem.*, 3, 344–356, <https://doi.org/10.1021/acsearthspacechem.8b00177>, 2019.
- Zheng, B., Zhang, Q., Zhang, Y., He, K. B., Wang, K., Zheng, G. J., Duan, F. K., Ma, Y. L., and Kimoto, T.: Heterogeneous chemistry: a mechanism missing in current models to explain secondary inorganic aerosol formation during the January 2013 haze episode in North China, *Atmos. Chem. Phys.*, 15, 2031–2049, <https://doi.org/10.5194/acp-15-2031-2015>, 2015.
- Zheng, Y., Chen, Q., Cheng, X., Mohr, C., Cai, J., Huang, W., Shrivastava, M., Ye, P., Fu, P., Shi, X., Ge, Y., Liao, K., Miao, R., Qiu, X., Koenig, T. K., and Chen, S.: Precursors and Pathways Leading to Enhanced Secondary Organic Aerosol Formation during Severe Haze Episodes, *Environ. Sci. Technol.*, 55, 15680–15693, <https://doi.org/10.1021/acs.est.1c04255>, 2021.
- Zheng, Y., Miao, R. Q., Zhang, Q., Li, Y. W., Cheng, X., Liao, K. R., Koenig, T. K., Ge, Y. L., Tang, L. Z., Shang, D. J., Hu, M., Chen, S. Y., and Chen, Q.: Secondary Formation of Submicron and Supermicron Organic and Inorganic Aerosols in a Highly Polluted Urban Area, *J. Geophys. Res.-Atmos.*, 128, e2022JD037865, <https://doi.org/10.1029/2022jd037865>, 2023.